

**STATISTICAL INVESTIGATION OF FATIGUE CRACK INITIATION AND GROWTH  
AROUND CHAMFERED RIVET HOLES IN ALCLAD 2024 T3  
AS AFFECTED BY CORROSION\***

M. I. Fadragas, M. E. Fine, B. Moran  
Center for Quality Engineering and Failure Prevention  
Northwestern University  
Evanston, IL

5/9-39  
23/13  
P. 19

**SUMMARY**

In panel specimens with rivet holes cracks initiate in the blunted knife edge of the chamfered rivet hole and propagate inward as well as along the hole. The fatigue lifetime to dominant crack formation was defined as the number of cycles,  $N_{500\mu\text{m}}$ , to formation of a 500  $\mu\text{m}$  long crack. Statistical data on  $N_{500\mu\text{m}}$  and on crack propagation after  $N_{500\mu\text{m}}$  were obtained for a large number of uncorroded specimens and specimens corroded in an ASTM B 117 salt spray. Considerable variation in  $N_{500\mu\text{m}}$  and crack propagation behavior was observed from specimen to specimen of the same nominal geometry and loading conditions. Statistical analysis of the data showed salt spray of Alclad 2024-T3 specimens with chamfered rivet holes increased the probability for both early formation and later formation of a propagating 500  $\mu\text{m}$  fatigue crack. The growth of fatigue cracks after 500  $\mu\text{m}$  size was little affected by prior salt spray.

**INTRODUCTION**

There is great variability in the fatigue behavior of any component even if the loading conditions are constant and this is due to many factors such as microstructure, surface finish, and environmental effects. The purpose of the present study was to assemble data sets on crack initiation, defined as the lifetime to a propagating 500  $\mu\text{m}$  long crack, and the Paris equation constants for propagation after 500  $\mu\text{m}$  crack length in samples of Alclad 2024-T3 aluminum alloy before and after exposure to ASTM B 117 salt spray with a 5% salt solution. The loading conditions were kept constant and the rivet holes were machined in a computer machine controlled tool. Statistical analysis of the data was performed. A small

---

\* This work was supported by the Federal Aviation Administration through the Center for Aviation Systems Reliability

but definite effect of corrosion was observed mainly in the initiation stage. Considerable variation in cycles to fatigue crack initiation and in the Paris equation constants was observed in all of the data sets.

## EXPERIMENTAL PROCEDURE

The material chosen for all the experiments was commercially available Alclad 2024-T3 aluminum alloy sheet. The sheet was 1.016 mm (0.040 in.) thick including an aluminum cladding thickness of 60  $\mu\text{m}$  (0.00236 in.) on both sides. All the specimens were made from a single sheet of material. The specimens used in this study were small panel specimens with single rivet holes. Figure 1 shows the specimen dimensions, rivet hole dimensions, rolling direction, loading direction, and gripping configuration of the specimens. The specimens were gripped using friction grips and had a length of 108 mm (4.25 in.) between the grip edges. The specimens were 38.1 mm (1.5 in.) wide and were loaded normal to the rolling direction of the sheet. The width of the specimens corresponds to the inter-rivet spacing and the loading direction is consistent with the major stress axis of in-service airplane fuselages (refs. 1 and 2).

Flush head type rivet holes shown in figure 2 were drilled using a computer machine controlled tool to ensure repeatability of the hole dimensions and drilling conditions. The rivet holes were drilled to specifications used in the airplane industry (refs. 3, 4 and 5). The rivet holes were made with a chamfered region that makes a  $100^\circ$  angle centered on the vertical. The rivet hole chamfer was drilled so that it penetrated through 80% of the thickness of the material, 0.813 mm (0.032 in.). The rivet hole chamfer depth was measured using a ball bearing and the depth was controlled to within 5.0  $\mu\text{m}$  (0.0002 in.). In actual industrial applications many of the rivet holes and chamfers are drilled by hand with a specialized tool. Considerably more variation in the rivet hole dimensions than that found in these experiments may be expected. Care was taken to accurately repeat the drilling process because the chamfered rivet holes tend to have a blunted knife edge (figure 2) that acts as a stress riser and a crack initiation site (refs. 1 and 6).

The tensile fatigue testing machine used was an MTS servo-hydraulic uniaxial fatigue apparatus System No. 821.74-01 which has a maximum capacity of 100 kN. All the tests were performed in ambient air at room temperature of 24  $^\circ\text{C}$ . The loading was done at 5 Hz with a saw-tooth wave generated by a function generator and verified with the use of a digital recording oscilloscope. The specimens were attached to the testing machine using friction grips. The grips were aligned with the use of a Wood's metal pot.

The nominal stress reported in all the plots of the data was calculated by dividing the applied load by the cross-sectional area of the specimen neglecting the rivet hole. The fatigue testing was done in load control with an R ratio of 0.1 and a maximum load of 4.0 KN. This load corresponds to a nominal stress  $S$  of 100 MPa (14.5 ksi) in the cross-section of the specimen.

An optical microscope with a 4X objective and a 10X eyepiece equipped with a measuring micrometer X-Y stage was used to observe fatigue crack formation and measure fatigue crack growth quantitatively. The crack length measurements made with the X-Y stage were repeatable within 5  $\mu\text{m}$ . The cracking that was observed around the rivet hole initially consisted of many small surface cracks. Later single cracks on each side of the hole became the dominant fatigue cracks. The fatigue crack lengths were measured on the blunted knife edge side of the specimen in-situ with the maximum load applied. The measurement was made from the edge of the rivet hole, where the fatigue crack initiated, to the crack tip.

In this study there were three batches of specimens. The three batches were cut from the same sheet of material but were fatigued and corroded in different ways from each other. The first batch was fatigued to fracture without any exposure to a corrosive atmosphere. The second batch was fatigued for 100,000 cycles, exposed to a corrosive atmosphere, and then fatigued to fracture. The third batch was exposed to a corrosive atmosphere prior to any cycling and then fatigued to fracture. The corrosive atmosphere used in this study was exposure to ASTM B 117 salt spray with a 5% salt solution for a period of 2 weeks. The specimens were then cleaned with deionized water and fatigued to fracture with intermittent crack length measurements.

Variability in the cycles to fatigue crack initiation is expected due to local variations in the surface finish of the hole caused by the drilling process as well as microstructural and chemical variations due to the processing of the material. The local variations in surface finish can be stress raisers such as burrs, machining marks, scratches, localized plastic deformation and particles in the material itself.

## RESULTS

In previous studies (refs. 7 and 8) it was found useful to separate the fatigue process from a chamfered rivet hole into two distinct parts in order to compare the variations from specimen to specimen. For this purpose the fatigue cycles to fracture were broken down into a crack initiation segment and a crack growth segment. The initiation segment is defined as the cycles to the initiation of a propagating fatigue

crack 500  $\mu\text{m}$  in length. The growth segment is defined as the cycles from the initiation of a propagating 500  $\mu\text{m}$  long fatigue crack to fracture of the specimen.

Using in-situ optical microscopy it was observed that many small surface fatigue cracks initiated at the blunted knife edge (figure 2) of the rivet hole during the fatigue cycling of the specimens. These surface cracks varied in length but most did not appear to grow once they were initiated. It is thought that microscopically the small surface cracks link up to form through cracks which propagated on both the front and rear surfaces of the panel specimens. Two such through cracks, one on either side of the rivet hole normal to the loading direction, formed in all of the specimens. These cracks were the dominant fatigue cracks and grew to fracture. It was observed that once a through crack reached 500  $\mu\text{m}$  in length it was identifiable as a dominant fatigue crack. Small cracks also formed ahead of the crack tip while the dominant fatigue cracks grew to fracture. The dominant fatigue cracks grow in part by joining up with the small cracks that form ahead of the crack tip.

The specimens that had been exposed to the salt spray formed a dominant fatigue crack on one side of the rivet hole many cycles before a dominant fatigue crack would form on the other side. This effect was observed to correlate with the fact that the fatigue specimens were placed upright on their sides while they were in the salt spray. The side that tended to first initiate a dominant fatigue crack coincided with the side that was lower in the salt spray and allowed more salt and water to collect on that side of the rivet hole.

The two cracks on each of the specimens were treated separately. Figures 3, 4 and 5 show the crack length ( $a$ ) vs. number of cycles ( $N$ ) curves for the three batches of specimens. The  $a$  vs.  $N$  data for each crack was curve fit to a least square exponential fit (eqn. 1) and the number of cycles to the initiation of a propagating 500  $\mu\text{m}$  long fatigue crack were determined for each crack.

$$a = a_0 e^{vN} \quad (1)$$

Figure 6 is a plot of the fraction of rivet hole sides in which a propagating 500  $\mu\text{m}$  long crack has not formed vs. the number of cycles ( $N$ ) for the three batches of specimens. The distribution of the data is wider for the two batches of specimens that were exposed to the salt spray. For the batch that was exposed to the salt spray prior to any cycling, the probability for earlier initiation of a propagating 500  $\mu\text{m}$  crack increased as well as the probability for later initiation as compared to the specimens that were not exposed to the salt spray. The same occurred for the batch exposed to salt spray after 100,000 cycles but to a lesser extent.

Empirical solutions for the stress intensity factor of a crack emanating from a chamfered rivet hole in a finite width specimen were not found in the literature. The  $\Delta K$  values used were estimated using a combination of two finite element method (FEM) solutions found in Murikami (ref. 9). This compound method does not take into account the three dimensional effect caused by the rivet hole chamfer but is still useful for determining an approximate  $\Delta K$  value for comparison purposes.

The first FEM solution for the stress intensity factor  $K$  was for two equal length cracks emanating from both sides of a circular hole in a finite width rectangular specimen. This solution was implemented to correct the  $\Delta K$  values for the finite width specimen and to correct for the cracks emanating from a hole. The solution called for a radius  $R$  and a crack length  $C$ . The radius for the non-chamfer part of the rivet hole was used for  $R$ . The value used for  $C$  was the average of the measured crack lengths of the cracks emanating from both sides of the rivet hole. The stress  $\sigma$  used in the calculation was corrected for the loss of load bearing material due to the rivet hole and the crack length. The empirical formula for the solution was provided by H. Fühling (ref. 10).

The second FEM solution for the stress intensity factor  $K$  was for a single crack in a finite width rectangular specimen that is off center from the specimen centerline. This solution was implemented to correct the  $\Delta K$  values for the difference in length of the two cracks emanating from the rivet hole. To avoid a double correction for a finite width specimen this solution was normalized so that only the relative magnitudes of the two  $K$  values were used. The solution called for a crack length  $C$  and the eccentricity  $E$ . The value used for  $C$  was the sum of the radius of the rivet hole and the average of the measured crack lengths of the cracks emanating from both sides of the rivet hole. The value used for  $E$  was calculated using the  $C$  value minus the radius  $R$  and the crack length on the opposite side of the specimen. The stress  $\sigma$  used in the calculation was corrected for the loss of load bearing material due to the rivet hole and the crack length. The empirical formula for the solution was provided by M. Isida (ref. 11).

The experiments were all performed with an  $R$  ratio of 0.1 thus the stress intensity range ( $\Delta K$ ) values were calculated using 90% of the maximum stress corrected for the loss of load bearing material due to the rivet hole and the crack length. Both the Fühling and Isida equations corrected for finite width specimens so the Isida equation was normalized to avoid a double correction for the finite width of the specimen. The final equation for  $\Delta K$  is as follows:

$\Delta\sigma$  = stress range corrected for loss of load bearing material and  $R$  ratio

$F(\Phi, \Psi)$  = Fühling  $\Delta K$  equation

$I_A(\alpha, \beta)$  = Isida  $\Delta K$  equation for crack A

$I_B(\alpha, \beta)$  = Isida  $\Delta K$  equation for crack B

$$\Delta K_A = \sqrt{\pi a} \Delta \sigma \cdot F(\Phi, \Psi) \cdot 2 I_A(\alpha, \beta) / (I_A(\alpha, \beta) + I_B(\alpha, \beta)) \quad (2)$$

(Führung eqn.)                      (normalized Isida eqn.)

The previously obtained exponential curve fit data for the a vs. N curves was used to calculate the crack growth rate (da/dN) for each point on the a vs. N plots (eqn. 3).

$$da/dN = v a_0 e^{vN} \quad (3)$$

Figure 7, 8 and 9 are the da/dN vs. ΔK plots for the three batches of specimens. The data from all three batches of specimens fit into a scatter band bounded by  $da/dN=9.26 \times 10^{-11} (\Delta K)^{3.33}$  on the top and  $da/dN=6.45 \times 10^{-12} (\Delta K)^{3.31}$  on the bottom.

## DISCUSSION

In deciding on inspection intervals the probability of early failure, of course, dominates. Salt spray prior to cycling has clearly increased the probability of early failure. It is not surprising that corrosion has increased the severity of defects responsible for crack initiation. The authors were surprised to find an increase in the long lifetime side of the distribution from the salt spray. There are specimens with relatively benign defects and perhaps minor cracks or flaws are filled with corrosion product and thus made less active. The effects of corrosion product in crack closure and in increasing the threshold stress intensity range for crack propagation is well known (ref. 12).

In order to more quantitatively compare corroded and non-corroded specimens the  $N_{500\mu m}$  data for the three batches of specimens were fit by the Weibull equation (eqn. 4).

$$\text{Percentage without } 500 \mu m \text{ cracks} = \exp[-(N/N_0)^{m_w}] \quad (4)$$

Figure 10 is the same plot as figure 6 with the exception that the data was fit to the Weibull equation with the number of cycles of loading (N) as the variable and the Weibull exponent  $m_w$  and  $N_0$  as the fitting parameters. The results of the curve fit are as follows for the three sets of specimens:

<u>Specimen Batch</u>	<u>N<sub>0</sub></u>	<u>m<sub>w</sub></u>
No Corrosion	145,944	4.776
Corrosion at 100,000 Cycles	144,692	5.842
Corrosion Prior to Cycling	133,908	4.234

The lower Weibull exponent is an indicator that the data for specimens which underwent corrosion prior to cycling has a more spread distribution of probabilities than that of specimens with no corrosion. The lower N<sub>0</sub> for pre-corroded compared to non-corroded specimens indicates that the 500 μm long dominant fatigue cracks initiated earlier in the pre-corroded batch of specimens in the low lifetime side of the distribution.

Salt spray after 100,000 fatigue cycles had much less of an effect than corrosion prior to any fatigue. Compared to the non-corroded specimens, the Weibull exponent is larger because the distribution was steeper in the mid-life regime; however, the Weibull coefficient is slightly smaller. The Weibull equation clearly fits these distributions only in the mid-range.

The cycles below which none of the specimens in a batch failed (i. e. the first data points in figures 6 and 10) are in the order corrosion at zero cycles, corrosion after 100,000 cycles, and no corrosion. This order is reversed in the plot regime where the probability of no 500 μm long dominant fatigue crack approaches zero.

Figure 11 is a plot of the Paris equation constant (C) vs. Paris equation exponent (m) that were derived from the da/dN vs. ΔK plots of figures 7, 8 and 9. The two parameters were derived by curve fitting the da/dN vs. ΔK data from each crack to the Paris equation (eqn. 5).

$$da/dN = C (\Delta K)^m \quad (5)$$

As discussed earlier the da/dN vs. ΔK data from all three batches of specimens fit into a relatively narrow scatter band bounded by da/dN=9.26x10<sup>-11</sup>(ΔK)<sup>3.33</sup> on the top and da/dN=6.45x10<sup>-12</sup>(ΔK)<sup>3.31</sup> on the bottom. As found in other metals there is a correlation of the C and m values. The data from each of the three batches of specimens were curve fit to an exponential equation (eqn. 6) and the results are as follows:

$$C = C_0 e^{\mu m} \quad (6)$$

<u>Specimen Batch</u>	<u>C<sub>0</sub></u>	<u>μ</u>
No Corrosion	1.8694e-08	-2.6843
Corrosion at 100,000 Cycles	2.4385e-08	-2.7748
Corrosion Prior to Cycling	1.6509e-08	-2.6635

These three curves are plotted in Figure 11 and there is little difference between them. The da/dN vs. ΔK curves were not significantly different for the three batches of specimens.

Figure 12 is a plot of the Paris equation exponent (m) vs. number of cycles to formation of a dominant 500 μm long crack (N<sub>500μm</sub>). The data for the three batches of specimens were curve fit to a line (eqn. 7). The results are as follows:

$$m = m_0 + s \cdot N_{500\mu m} \quad (7)$$

<u>Specimen Batch</u>	<u>m<sub>0</sub></u>	<u>s</u>
No Corrosion	1.5770	1.7615e-05
Corrosion at 100,000 Cycles	1.5022	1.7561e-05
Corrosion Prior to Cycling	-0.8340	4.2212e-05

In this data there was a slight upward trend of increase in m with N<sub>500μm</sub>, i.e. the cracks which initiated late in a number of cases grew more rapidly than the average.

In the three batches of specimens one crack would usually initiate earlier on one side of the specimen than on the other. On some occasions one crack would grow to several mm in length before a second dominant fatigue crack would appear on the other side of the specimen. This effect was more prevalent in the specimens that were exposed to salt spray either before cycling or after cycling for 100,000 cycles. The specimens were laid upright on their sides in the salt spray. This caused salt and water to deposit preferentially on the lower side of the rivet hole. In the salt sprayed specimens the side that tended to first initiate the dominant fatigue crack was the side where salt and water were deposited preferentially. This is further evidence that salt spray affects fatigue crack initiation.

1. Salt spray of Alclad 2024-T3 specimens with chamfered rivet holes increased the probability for early formation of a propagating 500  $\mu\text{m}$  fatigue crack.
2. A plot of probability for initiation of a propagating 500  $\mu\text{m}$  fatigue crack vs. cycles becomes more spread out from salt spray in both the high cycle and low cycle regimes.
3. The growth of fatigue cracks after 500  $\mu\text{m}$  size was little affected by prior salt spray.

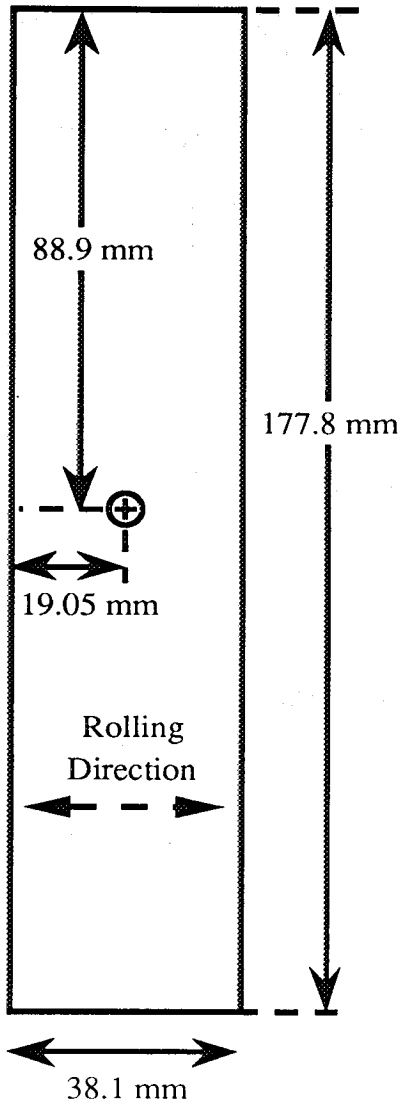
#### REFERENCES

1. Samavedam,G., Hoadley,D., Davin,J., "Test Facility for Evaluation of Structural Integrity of Stiffened & Jointed Aircraft Curved Panels", Springer Series in Computational Mechanics, Atluri, Sampath, Tong (Eds.), Structural Integrity of Aging Airplanes, Springer Verlag, Berlin Heidelberg, 1991, pp. 321-327.
2. Inventory of Foster-Miller Panels with attached Drawings, FAA, 29 NOV 91.
3. Installation, Inspection and Removal Methods for Aerolock 905, 906, 907 and 908 Rivets, H. D. Little Co., 10 SEPT 90.
4. Boeing 737 Structural Repair, Boeing Co., 1 FEB 69.
5. Boeing Part Standard, BACR15CE RIVET, 100<sup>o</sup> Shear Head, Boeing Co., 22 JUL 87.
6. Pelloux,R., Warren,A., O'Grady,J., "Fractographic Analysis of Initiation and Growth of Fatigue Cracks at Rivet Holes", Springer Series in Computational Mechanics, Atluri, Sampath, Tong (Eds.), Structural Integrity of Aging Airplanes, Springer Verlag, Berlin Heidelberg, 1991, pp. 293-308.
7. M. I. Fadrugas, "Tensile Fatigue Crack Initiation And Growth Database For Chamfered Rivet Holes In Alclad 2024-T3 Aluminum Alloy", M. S. Thesis, Northwestern University, OCT 1993.

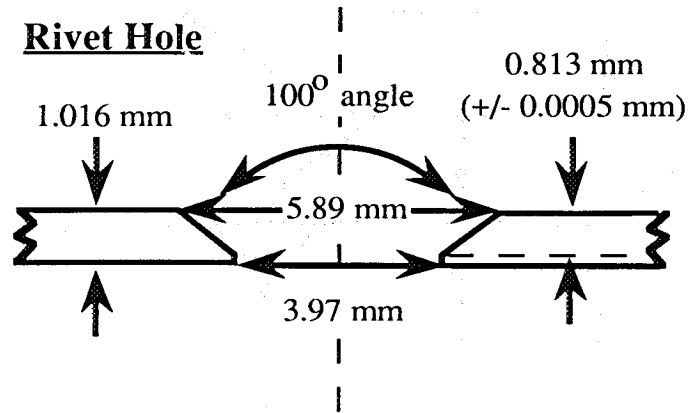
e-4.

8. "Tensile Fatigue Crack Initiation And Growth Database For Chamfered Rivet Holes In Alclad 2024-T3 Aluminum Alloy", Published as NAARP Report, Issue 3, JUL-OCT 1993, FAA Technical Center, Atlantic City International Airport, Atlantic City, NJ, 80405.
9. Murikami, Y., Stress Intensity Factors Handbook, Vol. 1, Pergamon Press, 1987, pp. 78-80, 291-297.
10. Führung, H., "Approximation Functions for K-Factors of Cracks in Notches", *Int. J. Frac.*, Vol. 9 (1973), pp. 328-331.
11. Isida, M., "Stress-Intensity Factors for the Tension of an Eccentrically Cracked Strip", *Trans. ASME, Ser. E, J. Appl. Mech.*, Vol. 33 (1966), pp. 674-675.
12. S. Suresh, G. H. Zaminski and R. O. Ritchie, "Oxide-Induced Crack Closure: An Explanation for Near-Threshold Corrosion Fatigue Growth Behavior", Metallurgical Transactions, 12A (1981) pp. 1435-1443.

### Specimen



### Rivet Hole



### Experimental Setup

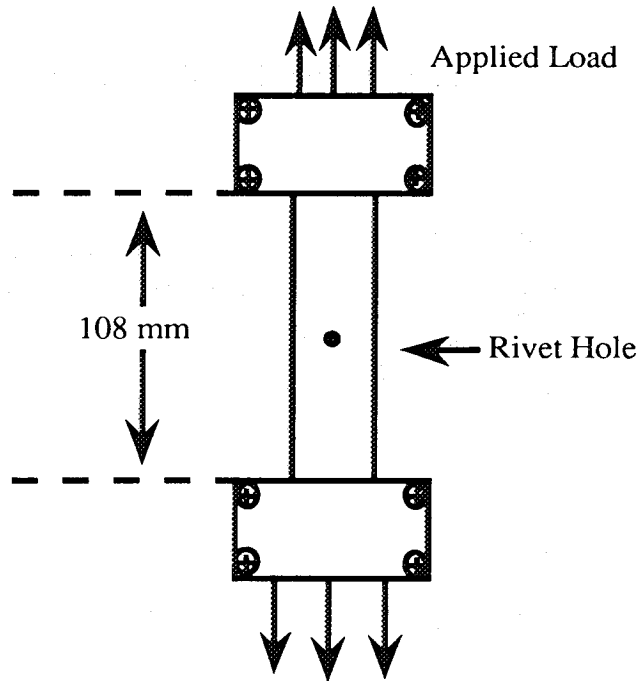


Figure 1. Specimen dimensions, rivet hole dimensions and experimental setup including loading and rolling directions.

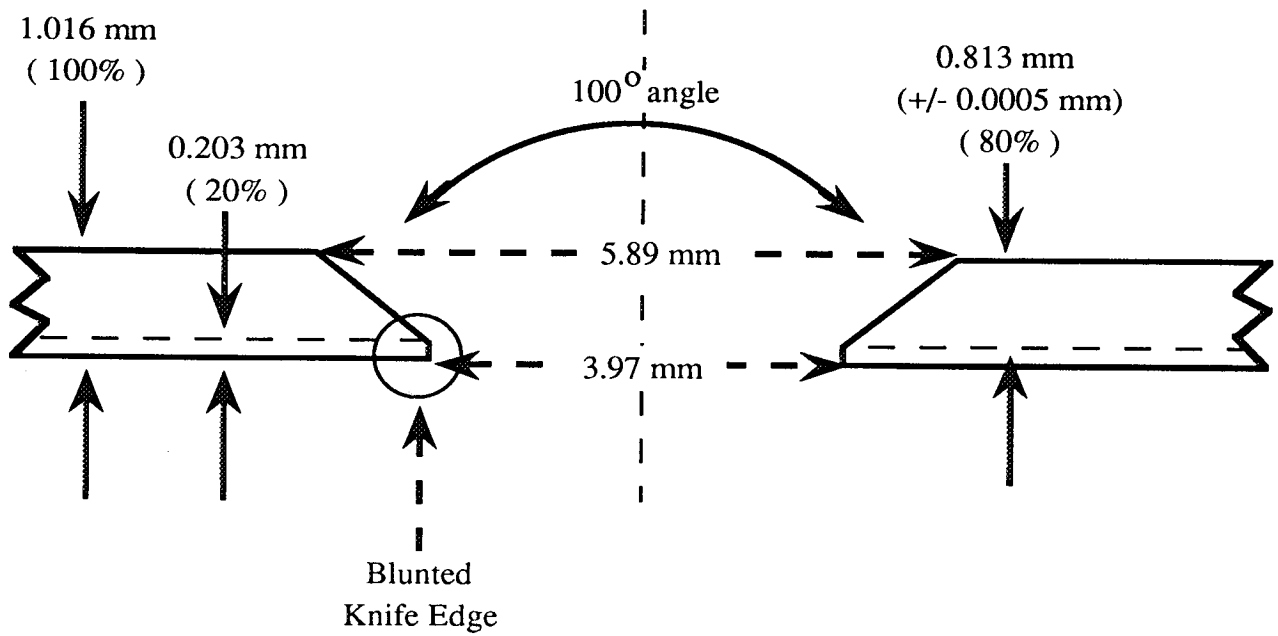


Figure 2. Rivet hole dimensions showing blunted knife edge.

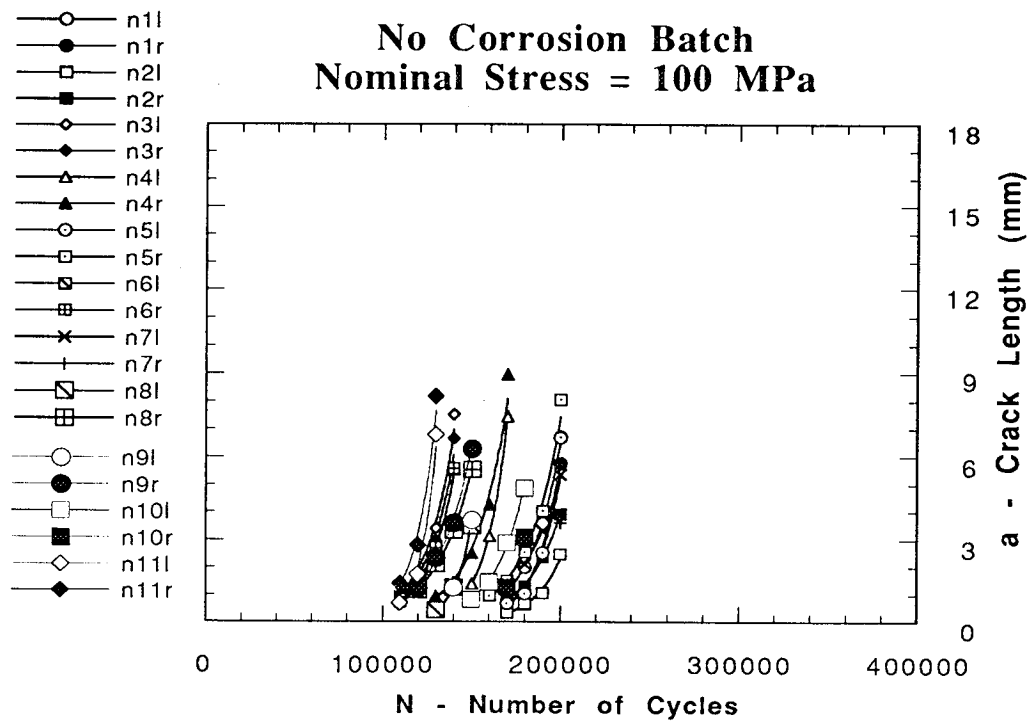


Figure 3. Crack length (a) vs. number of cycles (N) for specimens that were not exposed to salt spray.

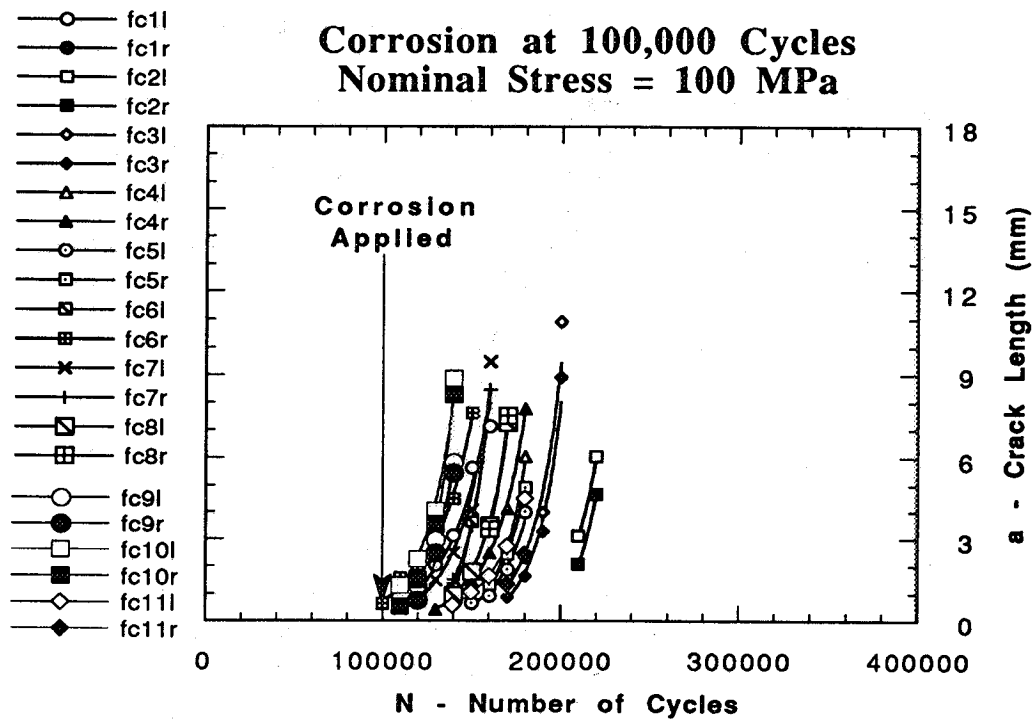


Figure 4. Crack length (a) vs. number of cycles (N) for specimens exposed to salt spray after 100,000 cycles.

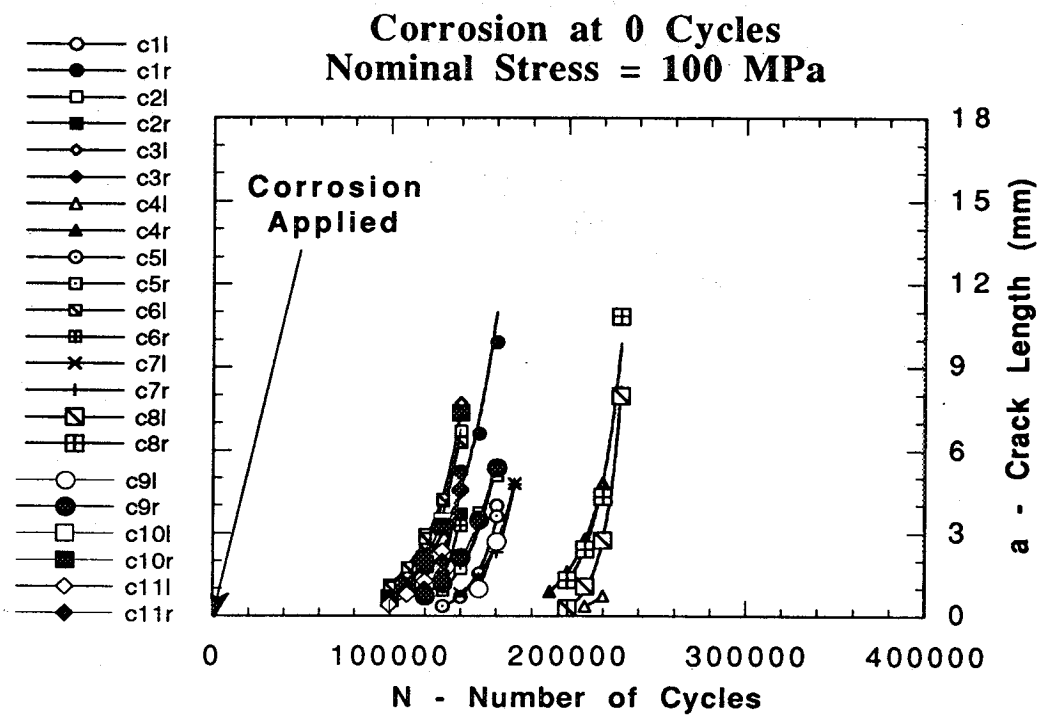


Figure 5. Crack length (a) vs. number of cycles (N) for specimens exposed to salt spray prior to cycling.

### Nominal Stress = 100 MPa

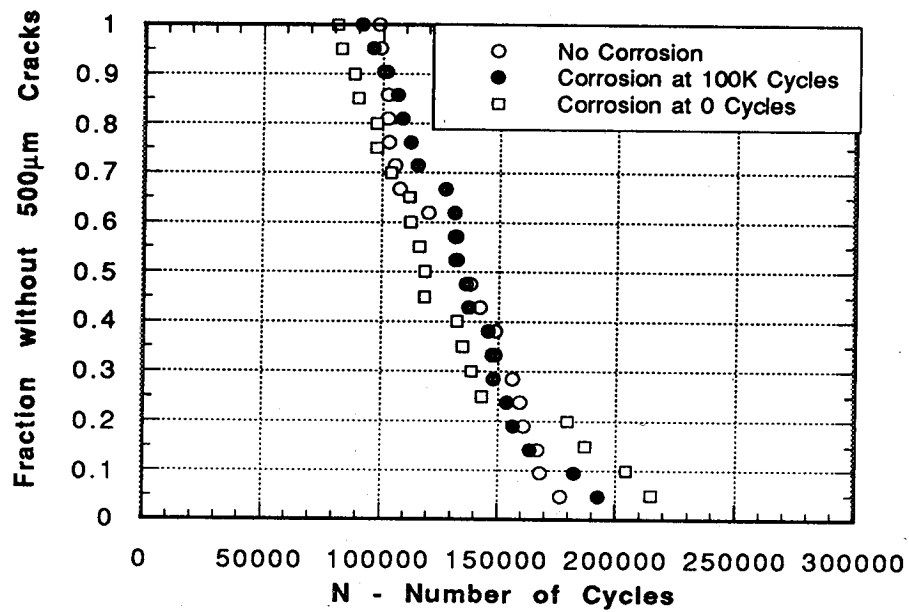


Figure 6. Fraction with no propagating 500 μm cracks vs. number of cycles (N).

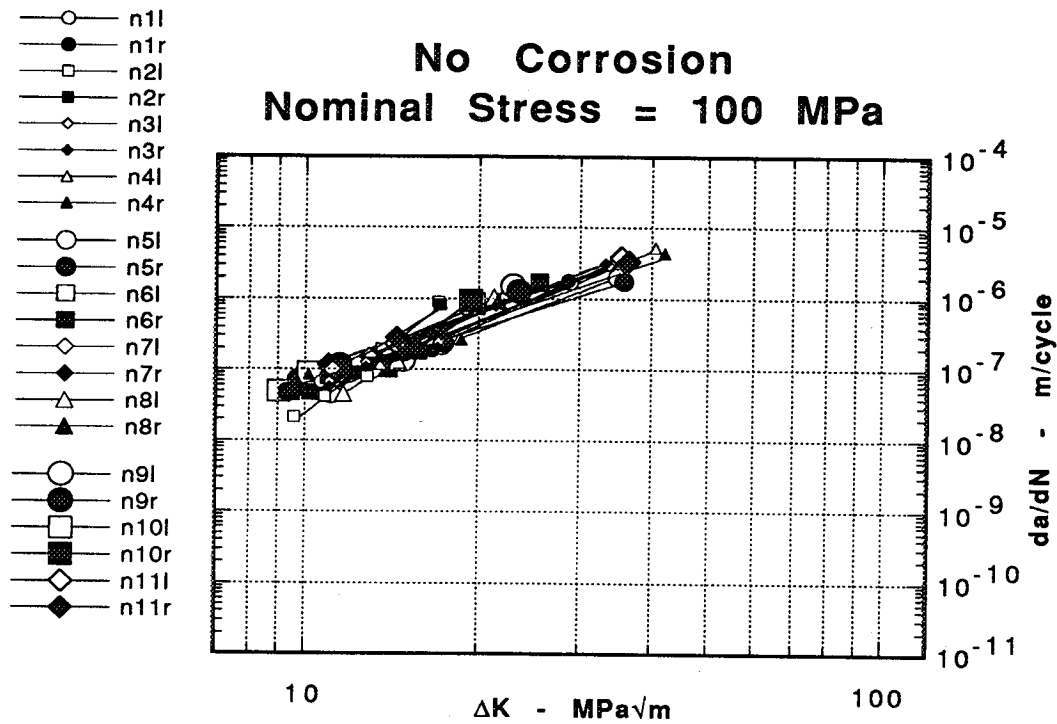


Figure 7. da/dN vs. ΔK for specimens not exposed to salt spray.

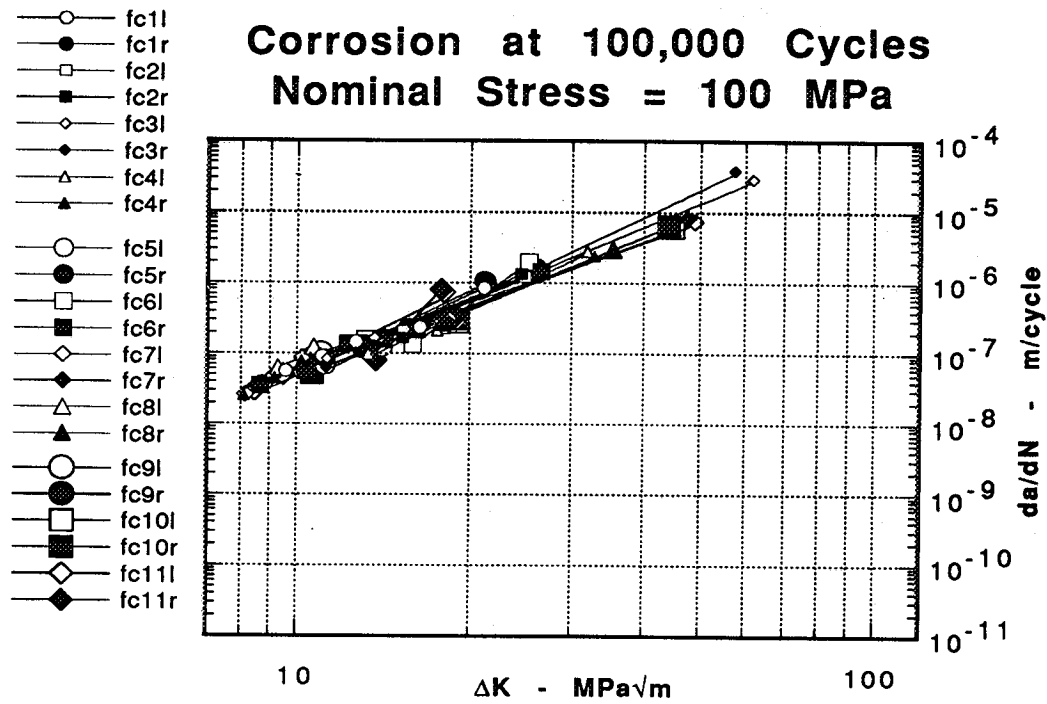


Figure 8.  $da/dN$  vs.  $\Delta K$  for specimens exposed to salt spray after 100,000 cycles.

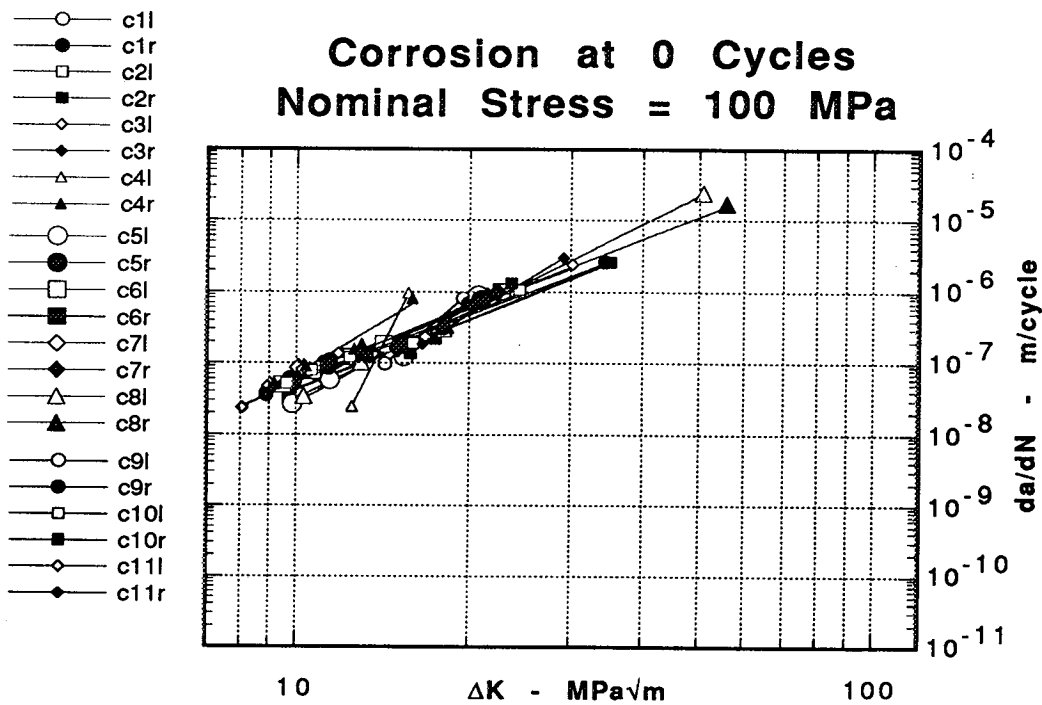


Figure 9.  $da/dN$  vs.  $\Delta K$  for specimens exposed to salt spray prior to cycling.

### Nominal Stress = 100 MPa

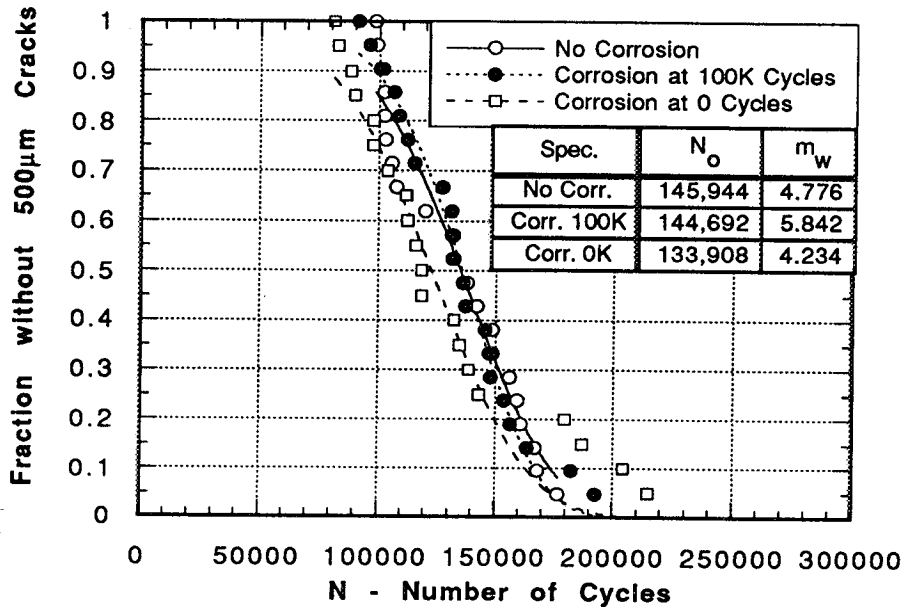


Figure 10. Fraction with no propagating 500 μm cracks vs. number of cycles (N) with curve fit to the Weibull equation.

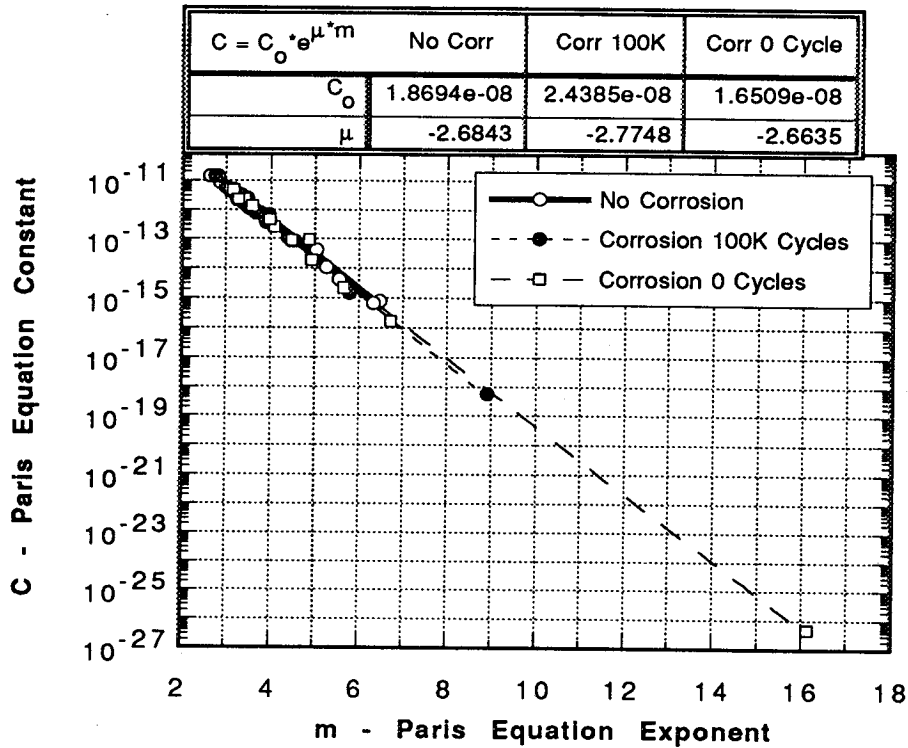


Figure 11. Paris equation constant (C) vs. Paris equation exponent (m).

Paris Equation Exponent (m) vs.  
Cycles to a propagating 500 $\mu\text{m}$  Crack ( $N_{500\mu\text{m}}$ )

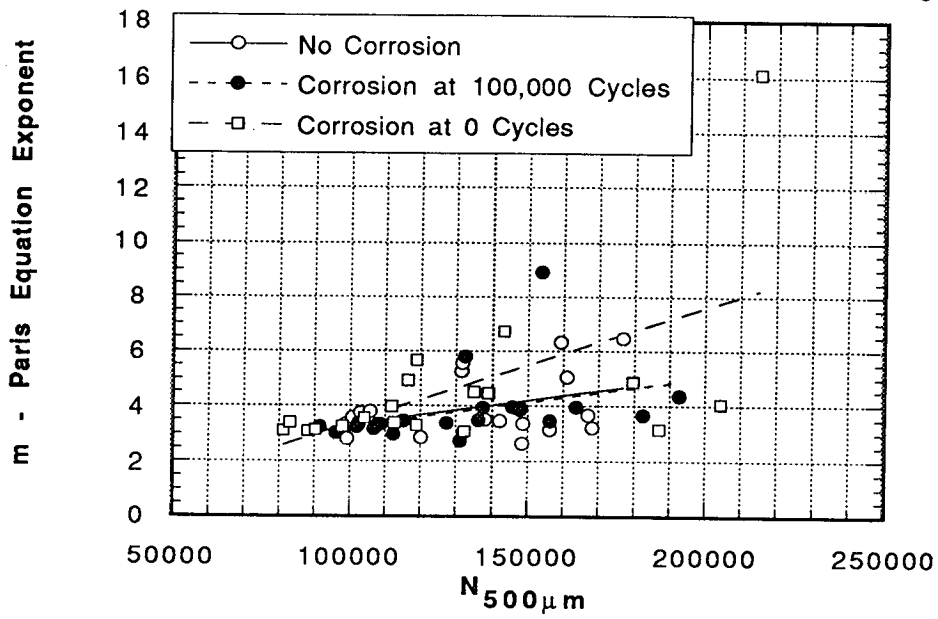


Figure 12. Paris equation exponent (m) vs. number of cycles to a propagating 500  $\mu\text{m}$  crack ( $N_{500\mu\text{m}}$ ).